J. Micromech. Microeng. **17** (2007) 1394–1401 doi:10.1088/0960-1317/17/7/023

A surface-micromachined vertical scanning micromirror

Ki Bang Lee[1] **and Liwei Lin**[2]

[1] KB Lab, 7 Rosewood Drive #10–13, Singapore 737937
[2] Berkeley Sensor and Actuator Center Department of Mechanical Engineering, University of California at Berkeley, CA, USA

E-mail: kblee@kblab.biz and kibanglee@hotmail.com

Received 3 January 2007, in final form 23 April 2007
Published 14 June 2007
Online at stacks.iop.org/JMM/17/1394

Abstract
A vertically supported, two-axial scanning micromirror with an optical reflection area of 600 μm $\times$ 600 μm has been successfully demonstrated using a 2 μm thick standard planar polysilicon surface micromachining process. The micromirror was lifted from the substrate and vertically supported by locking springs and hinges using a micromanipulator under a probe station. It was torsionally actuated in the two orthogonal angular directions including the first that is normal to the substrate and the second that is normal to the plane of the vertically supported microstructure. Furthermore, under an ac driving voltage of 2.5 V and dc bias voltage of 5 V, it was able to reflect and generate laser light patterns on a distant screen. The scanned and reflected laser light was able to make a circular pattern at $f = 387$ Hz, an elliptical pattern at $f = 350$ Hz and a line pattern at $f = 427$ Hz. As such, this surface-micromachined vertical mirror system could have potential applications for an optical bench on a chip.

(Some figures in this article are in colour only in the electronic version)

1. Introduction

Micromirrors are basic components in many optical systems such as scanners, microscopes, interferometers and waveguides. Both bulk- and surface-micromachining technologies [1–3] have demonstrated the feasibilities and potential of using micromirrors in scanning devices such as bar-code reading, optical data storage, telecommunication and display due to the inherent small inertia and fast response of these micromirrors. In previous demonstrations, torsional micromirrors have been used to scan light in a single axial direction with high operation bias voltages of 40 [1], 18 [2], 75 [3] and 40 V [4], respectively, and it is desirable to lower the operating voltages of these microdevices. In the area of two-axial actuators/mirrors, previous works include monolithic 2D actuators by means of thermal actuation [5], electromagnetic actuation [6] and electrostatic actuation [7–9]. These 2D mirrors are typically made using planar structures to have out-of-plane motions, while the scanning axes are parallel to the planar directions. It is interesting to investigate out-of-plane 2D scanning mirrors using surface-micromachining processes. Previously, a vertically supported two-axial comb drive [10] has been presented that allows vertically supported microstructures to be actuated in the directions parallel and normal to the comb fingers. This paper further presents a vertically supported micromirror that can scan in two axial directions under low operating voltages. Analyses and experiments on the electrostatic driving force and torque are presented with discussions on the design and two-axial scanning operations.

2. Theory and design

Figure 1 shows a schematic diagram of the two-axial torsional mirror that is vertically supported on a substrate by locking springs and hinges. Incident light is scanned and reflected in both θ and ϕ directions using the driving comb-structures. The micromirror is connected to beams that are supported on a substrate via hinges and locking springs. Left and right stationary combs are supported in the same manner. The comb structures of the micromirror and stationary comb structures are constrained on the substrate by the mechanical hinge structures [11]. The locking springs [10, 11] are

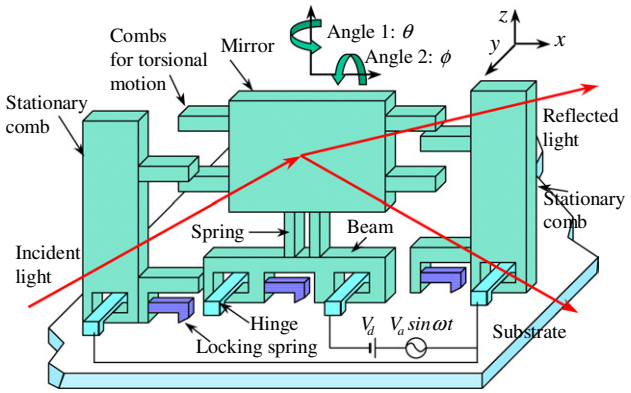

Figure 1. Schematic diagram of a vertically supported two-axial torsional micromirror: the mirror is vertically supported on the substrate by locking springs and hinges. Incident light can be scanned in the θ and ϕ angles using electrostatic torques generated by the comb actuators.

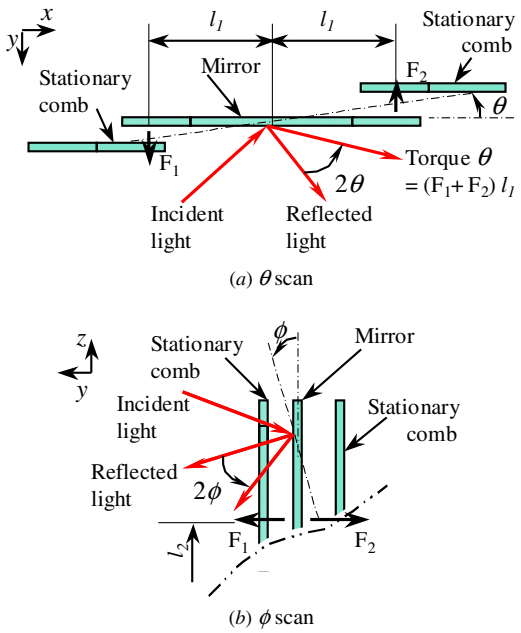

Figure 2. Comb placements in the x–y and y–z planes showing θ scan and ϕ scan: the electrostatic torques generated between combs move the mirror for θ and ϕ scans. Optical angles are twice the mechanical angles.

designed to play two important roles at the same time: (1) to supply adequate mechanical force on the hinge; (2) to assure good electrical contact between the ground plane and the vertically supported microstructures. All microstructures are first fabricated on the substrate and then lifted to the vertical position under a probe station in order to actuate the vertically supported micromirror in the θ and ϕ directions, as defined in figure 1. When a dc bias voltage, V_d, and ac driving voltage, V_a, are applied, electrostatic forces are generated between the stationary and movable combs and in turn provides the electrostatic torques in the θ and ϕ directions. Shown in figure 2(a) is a top view (normal to the z-axis) of the stationary comb and movable mirror arrangements to generate electrostatic torque for the θ scan. Figure 2(b) is a side view (normal to the x-axis) of the same arrangement to illustrate the

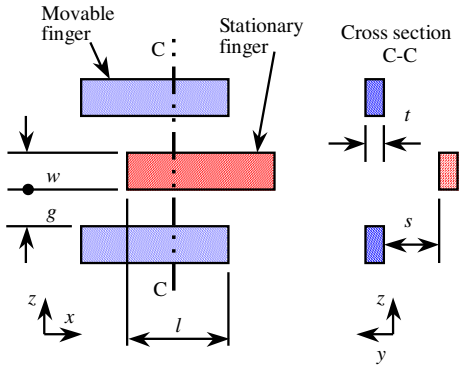

Figure 3. Comb finger configuration in the x–z and y–z planes. The gap, g, is controlled from the original mask design. The misalignment, s, is obtained during the vertical assembly process to generate the scanning torque.

electrostatic torque for the ϕ scan. The stationary combs are misaligned with the micromirror plate of about 12 and 24 μm respectively in this prototype setup to offer electrostatic torques for the θ and ϕ scans. A pair of forces, F_1 and F_2 in figures 2(a) and (b), acts on the mirror at l_1 and l_2 (a distance from the substrate to the center of the mirror) to generate moments for torsional motions. The optical scanning angle of the micromirror will be twice the mechanical angle.

In order to analyze the electrostatic force and torque in both x–z and y–z planes, figure 3 shows the relative positions of a pair of comb fingers. Movable and stationary fingers are interdigitated for electrostatic force in the x direction but misaligned by a distance, s, between movable and stationary fingers in the y direction to generate an electrostatic force in the y direction. The electrostatic force between fingers of the conventional comb structures [1–3] is theoretically obtained from the derivative of the electric field energy stored between the comb fingers. However, theoretical electrostatic forces of the comb fingers positioned, as shown in figure 3, cannot be derived analytically because of nonlinear behavior to the misalignment, s. The electrostatic force f_y on a pair of fingers of figure 3 is expressed from finite element analysis using a commercial code MAXWELL [12] as follows:

$$f_y = AlV^2 \tag{1}$$

where A, l and V are the force coefficients to be determined by numerical simulation, overlapping finger length and applied voltage, respectively. The force coefficient is not a constant but a function of the geometry of the finger width (w), the gap (g) between movable and stationary fingers and the finger thickness (t), as shown in figure 3. Table 1 summarizes the design parameters of a prototype two-axial torsional micromirror. A simulation using the software, MAXWELL, is conducted to obtain the electrostatic force coefficient, A, and figure 4 shows potential lines of the y–z plane in figure 3. The force coefficient A_1 of the left comb is estimated to be 3.3×10^{-7} N V^{-2} m^{-1} from this simulation for the prototype device with dimensions of $w = g = 3$ μm, $t = 2$ μm and $s = 12$ μm, respectively. For $w = g = 3$ μm, $t = 2$ μm and $s = 24$ μm, the force coefficient A_2 of the right comb is obtained to be 8.7×10^{-8} N V^{-2} m^{-1} from the simulation. The force coefficient can be approximated as $A = 6 \times 10^{-12}/s - 1.674 \times$

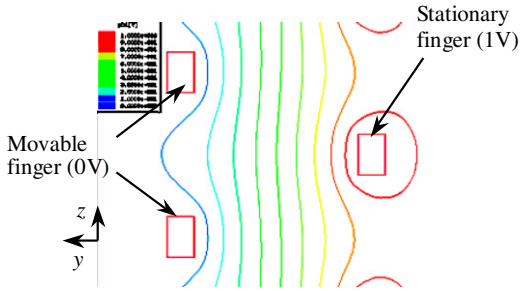

Figure 4. Equipotential line around movable and stationary fingers from MAXWELL simulation. The electrostatic force coefficient is estimated to be 3.3×10^{-7} N m^{-1} V^{-2} for dimensions of $w = g = 3$ μm, $t = 2$ μm and $s = 12$ μm.

Table 1. Designed parameters of the micromirror.

Structure material	Polysilicon
Mirror size	600 μm x 600 μm
Half height of the mirror, b	300 μm
Structure thickness, t	2 μm
Number of finger pairs, n	49 (each comb)
Distance to the combs, l_1	375 μm
Distance from substrate to mirror center, l_2	450 μm
Spring beam	
Length of spring beam, l_b	150 μm
Width, w_b	2 μm
Distance to spring beam, a	100 μm
Number of spring beam	2
Comb finger dimensions	
Gap, g	3 μm
Finger width, w	3 μm
Misalignment (left comb), s	12 μm
Misalignment (right comb), s	24 μm
Finger length	120 μm
Overlapping finger length, l	90 μm
Force coefficient (left comb), A_1	3.3×10^{-7} N m^{-1} V^{-2}
Force coefficient (right comb), A_2	8.7×10^{-8} N m^{-1} V^{-2}

10^{-7} for $s = 12 \times 10^{-6}$ m–24×10^{-6} m, where A and s are in N V^{-2} m^{-1} and m, respectively.

For the first-order approximation, it is assumed that the micromirror is a rigid body in the following analyses. When a voltage is applied across the movable structure and the stationary combs in figures 1 and 2, the electrostatic forces F_1 and F_2 are generated on the first and second combs as follows:

$$F_1 = nA_1lV^2 \tag{2}$$

$$F_2 = nA_2lV^2 \tag{3}$$

where n, A_1 and A_2 are the total number of comb pairs and the force coefficients for the first and second comb finger pairs, respectively. Figure 5 shows the forces acting on the micromirror. The first and second electrostatic forces F_1 and F_2 are applied at the distance l_1 from the center of the mirror and provide the θ and ϕ directional torsion of the mirror, respectively. Two spring beams supporting the micromirror resist the electrostatic forces. In figure 5, l_1, a, b, l_b, w_b and t denote the distance between the electrostatic force regions (center of the overlapping comb finger regions) and the center of the mirror, the half distance between the centers of the two

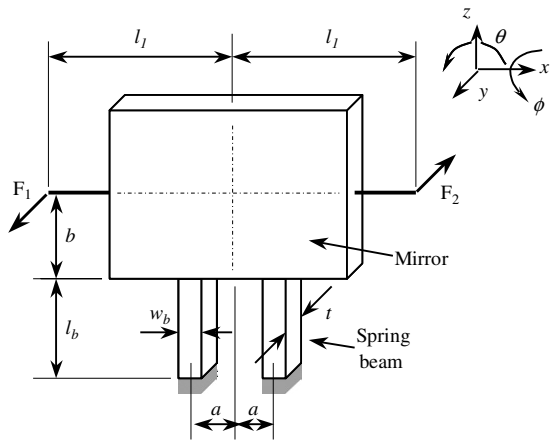

Figure 5. Electrostatic forces on the movable structure: F_1 and F_2.

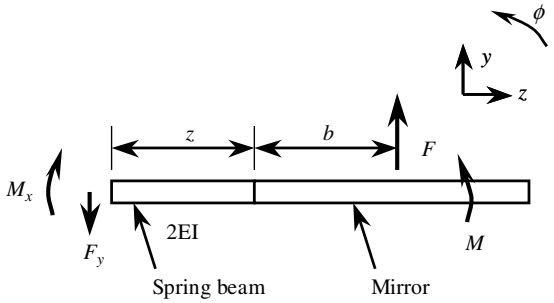

Figure 6. Free body diagram of the mirror and spring beam for operation in the ϕ direction. The spring beam of length l_b is cut at z for the free body diagram.

supporting spring beams that are designed to be symmetrical to the center of the micromirror, the half distance of the mirror height, the length, width and thickness of the supporting spring beam, respectively.

The rotational angles θ and ϕ, corresponding to the applied voltage V, can be obtained from Castigliano's theorem [13]. Figure 6 shows a free body diagram of the mirror and spring beam to obtain the angle ϕ. The mirror is subjected to the following net force in the y direction:

$$F = F_1 - F_2 = n(A_1 - A_2)lV^2. \tag{4}$$

The bending moment in the spring beam at z is obtained from the moment balance of the free body diagram (figure 6) as follows:

$$M_x = F(b + z) + M \tag{5}$$

where M is a dummy moment for moment balance in the free body diagram. The elastic energy stored in the two spring beams of length l_b is obtained with respect to the force F_x and moment M as follows:

$$U_1 = \int_0^{l_b} \frac{M_x^2}{2(2EI)}\,\mathrm{d}z = \int_0^{l_b} \frac{(F(b+z)+M)^2}{4EI}\,\mathrm{d}z \tag{6}$$

where E and I are Young's modulus and the moment of inertia of the supporting spring beam, defined as $w_b t^3/12$. Using Castigliano's theorem [13] yields the angle ϕ as a function of the applied force:

$$\phi = \left.\frac{\partial U_1}{\partial M}\right|_{M=0} = \frac{F}{4EI}((b + l_b)^2 - b^2). \tag{7}$$

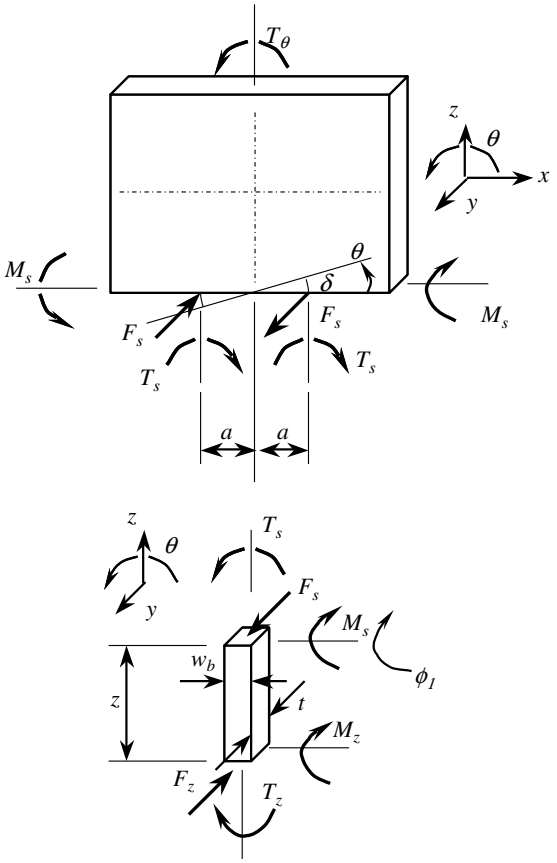

Figure 7. Free body diagram of the mirror and the spring beam for operation in the θ direction.

Similarly, the angle θ can be obtained from the derivative of a stored energy in the spring beams. Two free body diagram of figures 5 and 7 are used to obtain θ. In figure 7, the force F_s, the torque T_s and the bending moment M_s due to deformations of the spring beams keep balance with the applied torque T_θ in the θ direction that is generated from the two electrostatic force of figure 5. The torque on the mirror in figure 5 due to the electrostatic forces F_1 and F_2 is expressed as

$$T_\theta = (F_1 + F_2)l_1 = n(A_1 + A_2)ll_1V^2. \tag{8}$$

From figure 7, the balance of moment in the θ direction gives the following relation between the applied torque T_θ and the force F_s and torque T_s generated by the spring beams:

$$T_\theta = 2(F_s a + T_s) \tag{9}$$

where a is the distance measured from the center of the mirror to the spring beam. The free body diagram of figure 7 also gives the displacement of the end of the spring beam as a function of the angle θ:

$$\delta = a\theta. \tag{10}$$

The bending moment M_z and torque T_z at z of a spring beam are obtained from the moment balance of figure 8:

$$M_z = -M_s + F_s z \tag{11}$$

$$T_z = T_s. \tag{12}$$

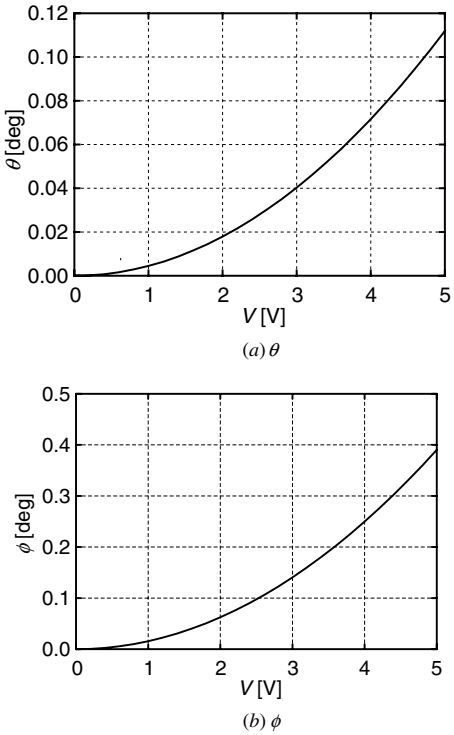

Figure 8. Analytical result of static angles θ and ϕ as a function of the applied dc voltage.

With the bending moment and the torque, the elastic energy stored in a beam is expressed as

$$U_2 = \int_0^{l_b} \left(\frac{M_z^2}{2EI} + \frac{T_z^2}{2GJ}\right)\mathrm{d}z = \int_0^{l_b} \left(\frac{(-M_s + F_s z)^2}{2EI} + \frac{T_s^2}{2GJ}\right)\mathrm{d}z \tag{13}$$

where G and J denote the shear modulus and the polar moment of inertia of the spring beam, respectively. Due to the fixed boundary condition at the connection of the supporting spring and the micromirror, the deflection angle at the end of the supporting spring in figure 7 is zero as follows:

$$\phi_1 = \frac{\partial U_2}{\partial M_s} = \int_0^{l_b} -\frac{-M_s + F_s z}{EI}\,\mathrm{d}z = \frac{1}{EI}\left(M_s l_b - \frac{F_s}{2}l_b^2\right) = 0. \tag{14}$$

The above equation yields the moment M_s with respect to F_s :

$$M_s = \frac{F_s}{2}l_b. \tag{15}$$

The displacement δ of the end of the spring beam is obtained with respect to the moment M_s and F_s:

$$\delta = \frac{\partial U_2}{\partial F_s} = \int_0^{l_b} \frac{-M_s z + F_s z^2}{EI}\,\mathrm{d}z = \frac{1}{EI}\left(-\frac{M_s}{2}l_b^2 + \frac{F_s}{3}l_b^3\right). \tag{16}$$

Substituting equation (15) into equation (16) yields δ as a function of the spring force F_s:

$$\delta = \frac{F_s}{12EI}l_b^3. \tag{17}$$

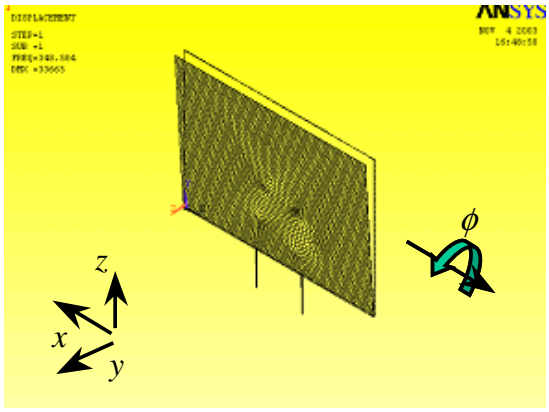

(*a*)

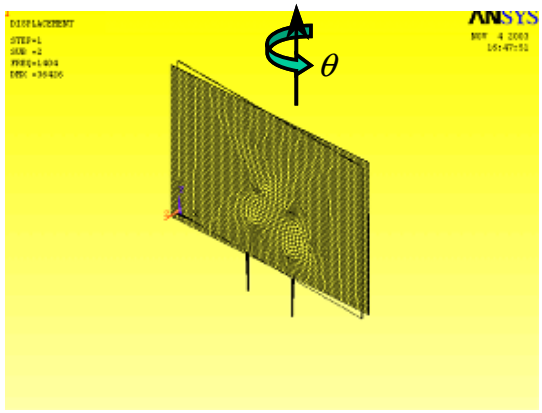

(*b*)

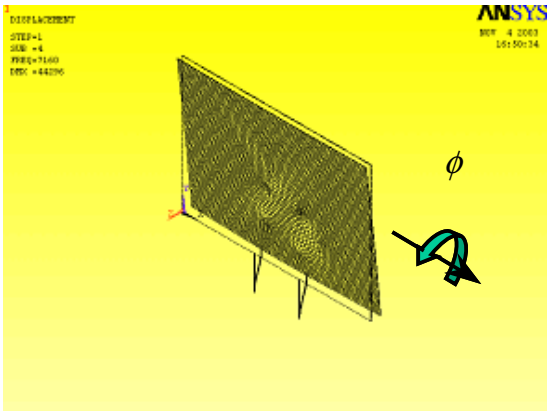

(*c*)

Figure 9. Modal analysis for the prototype device with dimensions listed in table 1. (*a*) Translation in the *y* direction; (*b*) angular motion in the θ direction; (*c*) angular motion in the ϕ direction. The resonant frequencies corresponding to modes (*a*), (*b*) and (*c*) are 581 Hz, 2.34 kHz and 11.93 kHz, respectively.

The angle θ of the spring beam in figure 7 is expressed as

$$\theta = \frac{\partial U_2}{\partial T_z} = \int_0^{l_b} \frac{T_s}{GJ}\,\mathrm{d}z = \frac{T_s l_b}{GJ}. \tag{18}$$

After substituting equations (17) and (18) into equation (9) and using the geometrical constraint equation (10), the angle θ

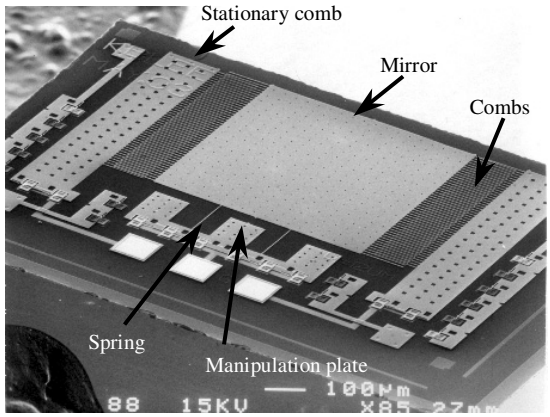

(*a*)

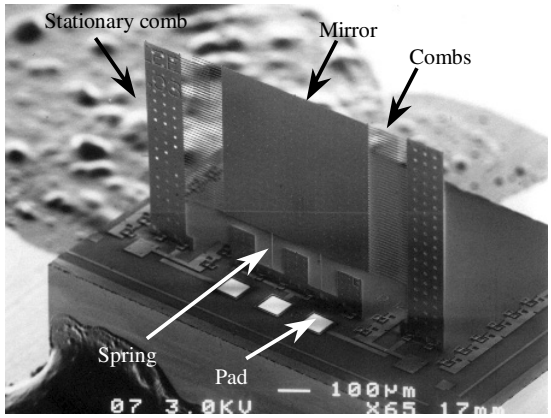

(*b*)

Figure 10. SEM photographs before and after being lifted from the substrate by using a micromanipulator: vertical structures are supported by locking springs and hinges and are electrically connected to electrical contact pads via hinges. The structure thickness is 2 μm. (*a*) Before lifted up; (*b*) after lifted up.

is expressed as a function of the applied torque T_θ.:

$$\theta = \frac{1}{2\left(\frac{12EI}{l_b^3}a^2 + \frac{GJ}{l_b}\right)} T_\theta. \tag{19}$$

The shear modulus for an isotropic material is defined as follows [13]:

$$G = \frac{E}{2(1+\nu)} \tag{20}$$

where E and ν represent Young's modulus and Poisson's ratio, respectively. For the supporting spring beam of $w_b \geqslant t$, the polar moment of inertial is expressed as [14]

$$J = t^3 w_b \left(\frac{1}{3} - 0.21\left(\frac{t}{w_b}\right)\left(1 - \frac{1}{12}\left(\frac{t}{w_b}\right)^4\right)\right). \tag{21}$$

For the rectangular beam of $w_b \leqslant t$, the following equation applies:

$$J = w_b^3 t \left(\frac{1}{3} - 0.21\left(\frac{w_b}{t}\right)\left(1 - \frac{1}{12}\left(\frac{w_b}{t}\right)^4\right)\right). \tag{22}$$

Substituting equation (8) into equation (19) gives the static angle θ that corresponds to the voltage V applied across the micromirror and the stationary combs:

$$\theta = \frac{1}{2\left(\frac{12EI}{l_b^3}a^2 + \frac{GJ}{l_b}\right)} n(A_1 + A_2) l l_1 V^2. \tag{23}$$

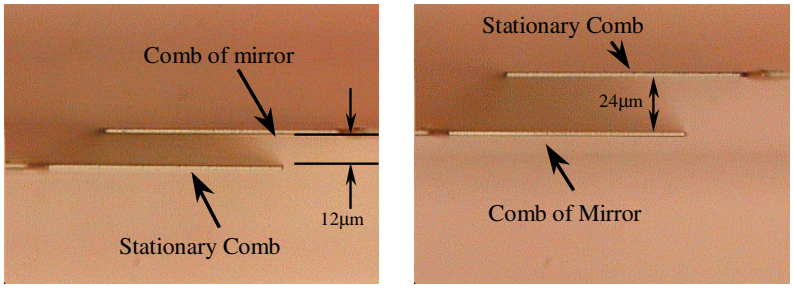

(*a*) (*b*)

Figure 11. Optical pictures of the top view of the lifted device showing misalignment of the stationary comb structures with the mirror plate —12 μm and 24 μm for the left and right stationary combs, respectively— to generate torque for θ and ϕ directional scans: (*a*) left comb; (*b*) right comb.

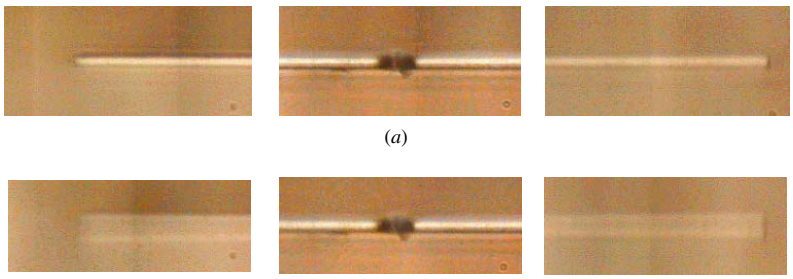

(*a*)

(*b*)

Figure 12. Optical pictures of the left, center and right portions of the micromirror: (*a*) no movement before actuation; (*b*) under an ac driving voltage of 2.5 V at 2007 Hz and dc bias voltage of 5 V. It is clear that the micromirror is vibrating in the θ direction since the center of the mirror does not move. (*a*) Before actuation; (*b*) after actuation.

Combining equations (7) and (14) yields the angle ϕ corresponding to the applied voltage V:

$$\phi = \frac{(b + l_b)^2 - b^2}{4EI} n(A_1 - A_2) l V^2. \tag{24}$$

Figure 8 shows results of θ and ϕ based on the above derivations using the data in table 1. It is observed in figure 8 that the angle θ and ϕ are a function of proportional to the square of the applied voltage. Furthermore, under a dc bias of 5 V, the angular deflections in the θ and ϕ directions are 0.11° and 0.4°, respectively.

When a dc bias voltage, V_d, and ac driving voltage, V_a, are applied, as shown in figure 1, the mirror vibrates under forced vibration due to the electrostatic force. Because the micromirror of figure 1 is a nonlinear vibration system of more than three degree-of-freedom, it is difficult to obtain the theoretical or analytic dynamic responses. However, one can conduct modal analysis to investigate mode shapes and corresponding resonant frequencies. Figure 9 shows the simulation results of possible mode shapes corresponding to force and torque on the mirror using a finite element analysis software, ANSYS [15]. The resonant frequencies corresponding to modes (*a*), (*b*) and (*c*) are 581 Hz, 2.34 kHz, and 11.93 kHz, respectively.

For a feasibility study of the two-axial scanning micromirror vertically supported by spring beams, the initial structure of table 1 is selected. The gap and width are selected to be 3 μm because the dimension can be easily defined in the surface micromachining using polysilicon [16]. In order to make two axial motions, the left misalignment is selected to be 12 μm and the right misalignment is 24 mm that is twice the left misalignment.

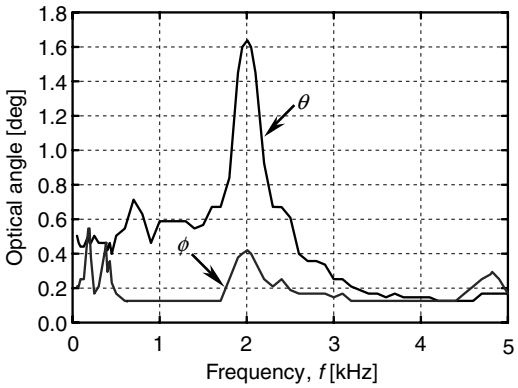

Figure 13. Optical angle under an ac driving voltage of 2.5 V and dc bias voltage of 5 V.

3. Results and discussion

Two-axial torsional micromirrors have been fabricated by the standard surface micromachining process [16]. Figure 10(*a*) shows a SEM photograph of the 2 μm thick micromirror before it is vertically lifted and supported. The manipulation plate in figure 10(*a*) is used to lift up the micromirror. Figure 10(*b*) shows a SEM photograph of the micromirror after being lifted from the substrate using a probe under a probe station. Vertical structures are supported by locking springs and hinges and are

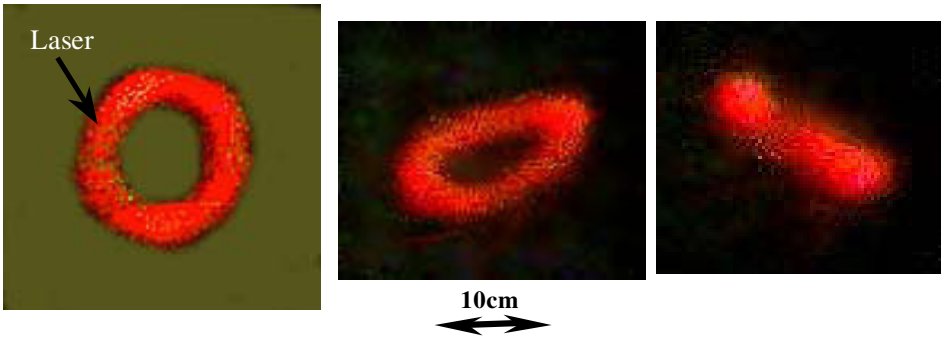

Figure 14. Patterns on a distant screen showing the effects of the combination of θ and ϕ scanning. The laser light is reflected by the moving micromirror to make a circle at $f = 387$ Hz, an ellipse at $f = 350$ Hz and a line at $f = 427$ Hz while the mirror is vibrating under an ac driving voltage of 2.5 V and dc bias voltage of 5 V.

electrically connected to contact pads via the hinges. The reflection area of the micromirror is 600 μm $\times$ 600 μm. The lifted structure is electrically connected to the electrode on the substrate when the locking spring deformed. The contact resistance between pads and the lifted structures is measured to be 11 kΩ. Figure 11 depicts a top view of the device showing the detail placement. Within an error of microscope resolution, the stationary combs are misaligned with the micromirror plate with 12 μm and 24 μm, respectively to generate the electrostatic force and torques for θ and ϕ scans.

The fabricated micromirror was observed to actuate under atmospheric pressure with an ac driving voltage of 2.5 V and dc bias voltage of 5 V. Figure 12(a) shows the left, middle and right portions of the mirror that do not move before applying the voltages, and figure 12(b) shows that the mirror is torsionally vibrating at the resonant frequency of 2007 Hz in the θ direction since the center portion of the micromirror plate is not moving. The measured vibration amplitude of the end of the polysilicon mirror is 6 μm. Without operating the device under resonance, it is possible to control the two-axial torsional micromirror to display various patterns by varying the input frequencies. Figure 13 shows optical angles in the θ and ϕ directions measured from the micromirror. The maximum optical angles are 1.64° and 0.42 ° in the θ and ϕ directions, respectively. The resonant frequency is 2.0 kHz that is a little lower than the theoretical predicted value of 2.34 kHz and the quality factor for θ scanning is estimated to be 6.5 from the experimental frequency spectrum. As seen in figure 10, the mirror has small-size etch holes to reflect much light and these small size holes on the mirror cause large damping force or low quality factor of 6.5. Figure 14 shows patterns generated by the two-axial torsional micromirrors, including circle, ellipse and line patterns on a distant screen (175 cm away from the micromirror). The laser light is reflected by the micromirror to make a circle at 387 Hz, an ellipse at 350 Hz and a line pattern at 427 Hz while the mirror is moving under an ac driving voltage of 2.5 V and dc bias voltage of 5 V. It is noted that the response at 350, 387 and 427 Hz are around resonant frequency in the ϕ direction to show that the mirror can make several patterns. The quality factor in the ϕ direction resonance is measured to be about 3. The resonant frequency in the θ direction is 2007 Hz with the quality factor of 6.5, as shown in figure 13, and the mirror at this frequency makes a line on the screen. The frequency response of the mirror in figure 13 suggests that the dynamic behavior in the ϕ direction is weakly coupled with that in the θ direction. The experimental resonant frequency of 2007 Hz in the θ direction in figure 13 corresponds to that (2340 Hz) of mode shape in figure 9(b). One of the resonant frequencies of 387 Hz and 194 Hz corresponds to the simulated frequency of figure 9(a). The simulated resonant frequency of 11.93 kHz was not observed in the experiment. It is noted that the measured resonant frequencies are lower than the simulated resonant frequencies. The lower resonant frequency suggests that the electric stiffness due to the electrostatic force may be comparable to the stiffness of the spring beams. Although the static responses in figure 8 briefly show the mirror behaviors, the real response includes resonance, as shown in figure 13. Therefore, the static responses of figure 8 cannot be directly compared with the measured data of figures 13 and 14. In order to optimize the performance of the mirror, further research on the dynamic behaviors needs to be performed. These preliminary demonstrations show the possibilities and feasibilities of applying these vertical scanning mirrors for applications in micro optical systems such as scanners, interferometer and bar-code reading.

4. Conclusions

We have successfully demonstrated and operated a vertically supported, two-axial torsional micromirror fabricated by the standard surface-micromachining process and assembled under a probe station. The 2 μm thick polysilicon micromirror, vertically supported on a substrate by locking springs and hinges, was torsionally actuated in the two orthogonal angular directions under ac driving voltage of 2.5 V and dc bias voltage of 5 V. It is found that reflecting laser light patterns under the controlled motion of the micromirror can generate patterns of line, ellipse or circle on a distant screen using various driving frequencies. Theoretical analyses on the electrostatic force and torque are conducted and supported by finite element analyses. The experimental measurements show that the maximum optical angles are 1.64° and 0.42° in the θ and ϕ directions at 2.0 kHz, respectively. The easy implementation of the system using standard surface-micromachining from various foundry services and low operation voltages provides opportunities to apply this new class of actuator in making optical systems on a chip.

References

[1] Kiang M-H, Solgaard O, Lau KY and Muller R 1998 Electrostatic combdrive-actuated micromirrors for laser-beam scanning and positioning *IEEE/ASME J. Microelectromech. Syst.* **7** 27–37

[2] Lee J-H, Ko Y-C, Kong D-H, Kim J-M, Lee K B and Jeon D-Y 2002 Design and fabrication of scanning mirror for laser display *Sensors Actuators* A **96** 223–30

[3] Krishnamoorthy U, Lee D and Solgaard O 2003 Self-aligned vertical electrostatic combdrives for micromirror actuation *J. Microelectromech. Syst.* **12** 458–64

[4] Kim J, Choo H, Lin L and Muller R S 2006 Microfabricated torsional actuators using self-aligned plastic deformation of silicon *IEEE/ASME J. Microelectromech. Syst.* **15** 553–62

[5] Schweizer S, Cousseau P, Lammel G, Calmes S and Renaud Ph 2000 Two-dimensional thermally actuated optical microprojector *Sensors Actuators* A **85** 424–9

[6] Asada N, Matsuki H, Minami K and Esashi M 1994 Silicon micromachined two-dimensional galvano optical scanner *IEEE Trans. Magn.* **30** 4647–49

[7] Hao Z, Clark R, Hammer J, Whitley M and Wingfield B 2002 Modeling air-damping effect in a bulk micromachined 2D tilt mirror *Sensors Actuators* A **102** 42–48

[8] Schenk H, Durr P, Kunze D, Lakner H and Kuck H 2001 A resonantly excited 2D-micro-scanning-mirror with large deflection *Sensors Actuators* A **89** 104–11

[9] Kim J, Christensen D and Lin L 2005 Monolithic 2-D scanning mirror using self-aligned angular vertical comb drives *IEEE Photon. Technol. Lett.* **17** 2307–2309

[10] Lee K B and Lin L 2005 Vertically supported two-directional comb drive *J. Micromech. Microeng.* **15** 1439–45

[11] Pister K S J, Judy M-W, Burgett S-R and Fearing R-S 1992 Microfabricated hinges *Sensors Actuators* A **33** 249–56

[12] *Getting Started: A 2D Electrostatic Problem* 2002 http://www.ansoft.com, Ansoft Corporation

[13] S H Crandall and N C Dahl 1987 *An Introduction to the Mechanics of Solids* 2nd edn (New York: McGraw-Hill)

[14] Young W C 1989 *Roark's Formulas for Stress and Strain* (New York: McGraw-Hill)

[15] Saeed M 2003 *Finite Element Analysis: Theory and Application with ANSYS* 2nd edn (Englewood Cliffs, NJ: Prentice-Hall)

[16] Carter J, Cowen A, Hardy B, Mahadevan R, Stonefield M and Wilcenski S 2006 *PolyMUMPs Design Hand Book* Revision 11.0 (MEMSCAP) http://www.memsrus.com

[17] Tang W C, Nguyen T-C H and Howe R T 1989 Laterally driven polysilicon resonant microactuators *Sensors Actuators* **20** 25–32